www.czasopisma.pan.pl PAN POLSKA AKADEMIA NAUK www.journals.pan.pl

Arch. Metall. Mater., Vol. 61 (2016), No 2, p. 635–640

DOI: 10.1515/amm-2016-0108

SANGHOON KIM*, HYUP JAE CHUNG**, KYONGYOP RHEE *,#

APPLICATION OF IMAGE PROCESSING TO PREDICT COMPRESSIVE BEHAVIOR OF ALUMINUM FOAM

An image processing technique was used to model the internal structure of aluminum foam in finite element analysis in order to predict the compressive behavior of the material. Finite element analysis and experimental tests were performed on aluminum foam with densities of 0.2, 0.25, and 0.3 g/cm^3. It was found that although the compressive strength predicted from the finite element analysis was higher than that determined experimentally, the predicted compressive stress–strain curves exhibited a tendency similar to those determined from experiments for both densities. However, the behavior of the predicted compressive stress–strain curves was different from the experimental one as the applied strain increased. The difference between predicted and experimental stress–strain curves in a high strain range was due to contact between broken aluminum foam walls by the large deformation.

Keywords: Aluminum foam, Compute tomography (CT) image, Finite element method (FEM)

1. Introduction

Metal foams are newly developed and functional materials that have low density, high specific strength, and excellent energy absorption [1–4]. Metal foams are environmentally friendly because they are easily recycled [5–6]. Metal foams are divided into open-cell and closed-cell types, depending on the shape of the cell in their structure. Accordingly, many studies have been carried out in order to understand the elastic modulus, tensile and compressive strength, buckling, and fracture behavior of various metal foams [7–12].

In recent years, many researchers have concentrated on using the finite element method to study the mechanical behavior of aluminum foam. The famous Gibson–Ashby model and numerical analysis based on a regularly periodic array of cells might be typical examples [13]. Konstaintinidis et al. [14] developed a three-dimensional (3D) model to account for the different cell geometry of aluminum foams, such as circular, elliptical, rectangular, and square. They also studied the elastic modulus and plateau stress according to cell geometries. Kenesei et al. [15] reported that analytical and numerical descriptions have been developed and compared with the results of compression tests in order to increase the plateau stress of metal foams. Both uniform and non-uniform cell-size distributions have been investigated. The energy absorption properties were also studied. Sassov et al. [16] showed that non-destructive 3D reconstruction and measurement of the internal micromorphology of foam structures offer new perspectives for standardization of such structures. Also, 3D quantitative parameters obtained through a micro-computed tomography (CT) investigation can be used in correlation with physical properties as a base for creating foam materials with predefined characteristics. Ohgaki et al. [17] explored the compressive and damage behavior of aluminum foams. Using the local tomography technique and an in-situ test rig, the relationship between microstructural features and fracture behavior were assessed by 3D local strain mapping. Yan Liu et al. [18] reported an empirical formula for dynamical plateau stress that was fitted with the calculated results. It is shown that the strain-rate effect and the relative density will increase the plateau stress by using 2D images. However, a few researchers have used a 3D numerical model of actual aluminum foam to analyze the foam.

In this study, the CT image from an X-ray imaging technique was used to model the internal structure of aluminum foam in finite element analysis in order to predict the compressive behavior of aluminum foam. Finite element analysis and experimental tests were performed on aluminum foam with densities of 0.2, 0.25, and 0.3 g/cm3. The predicted compressive behaviors were compared with those determined from the compressive tests.

2. Experimental

2.1. Compressive test

The materials used in this study were aluminum foam with densities of 0.2, 0.25, and 0.3 g/cm^3. The aluminum foam was cut into plates for compressive tests; each plate was 20 mm long, 70 mm wide, and 30 mm thick. A universal testing machine was used to carry out compressive tests at room temperature by applying displacement control at a rate of 3 mm/min. At least five tests were performed to ensure the reliability of the test results.

* DEPARTMENT OF MECHANICAL ENGINEERING, KYUNGHEE UNIVERSITY, YONGIN, KOREA

** CAE TECHNOLOGY GROUP, PRODUCTION ENGINEERING CENTER, LS CABLE 27,GONGDAN-RO 140BEON-GIL, GUNPO-SI, GYEONGGI-DO 453-831 KOREA

Corresponding author: rheeky@khu.ac.kr

2.2. Modeling and analysis

Computed tomography images of aluminum foams were used to obtain detailed depictions of aluminum foam for the 3D model. CT scanning was carried out using a CT system (Ray Scan 250, HWM, Germany), and an X-ray source of 225 kV and 2 mA was used. The tomography resolution was 300 μm. By detecting the edges of the images, a 3D graphic image was developed from the CT image slices by using CANTIBIO (Bionix BodyBuilder 3.36). A 3D finite element model of the aluminum foam was developed with ABAQUS/CAE (Dassault Systems Simulia Corp., U.S.A.), which allows for pre/post processing of finite element analyses. The model was divided into two parts according to the lightness and darkness of the CT images as aluminum and cell by controlled threshold through the segmentation process in Fig. 1. The segmented CT images were then stacked to form a 3D volume model of the aluminum foam in Fig. 2. This finite element model was developed using tetrahedron elements. A total of 100,000–250,000 nodes and 400,000–800,000 elements were used to mesh the model according to density in Fig. 3. Contact conditions were then applied using a general contact method. The boundary conditions were that the bottom plane was fixed in all directions (X, Y, and Z displacements and rotations) and the top plane was fixed except the load direction. A commercial software package, ABAQUS (Dassault Systems Simulia Corp., U.S.A.) was used for analysis of this model in order to compare it with the experimental results. Fig. 4 shows a flow chart for modeling and analysis of the aluminum foam.

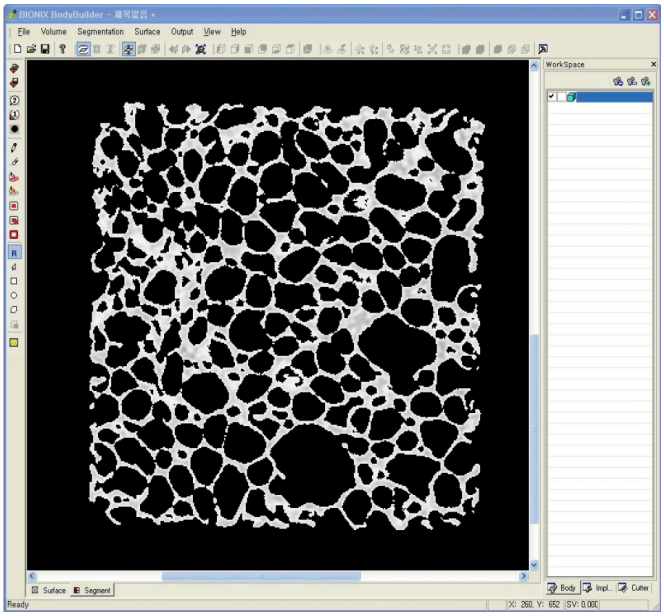

Fig. 1. Typical CT image segmented by controlling threshold

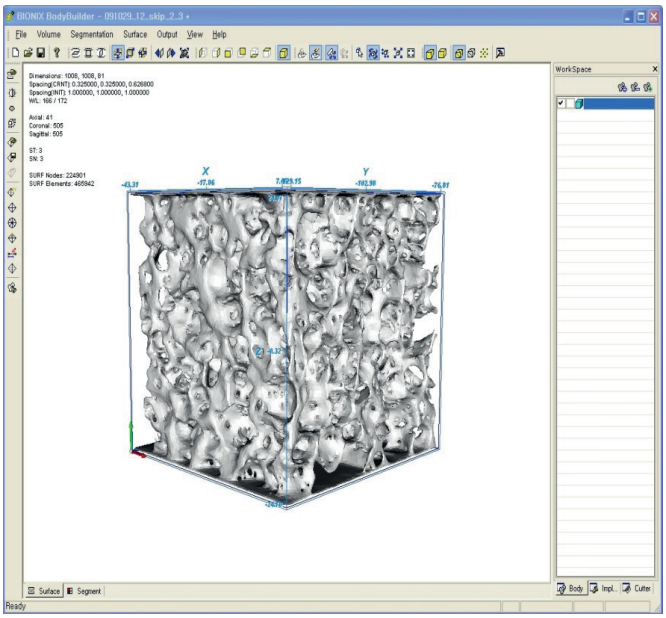

Fig. 2. Stacked CT images of aluminum foam

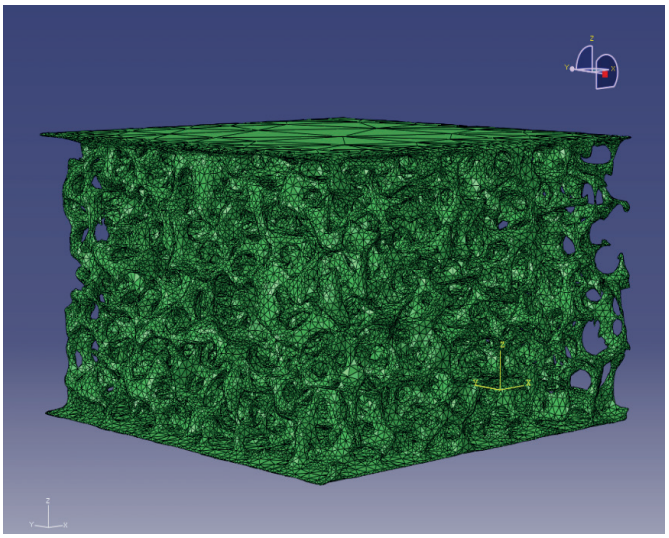

Fig. 3. Aluminum foam 3D model

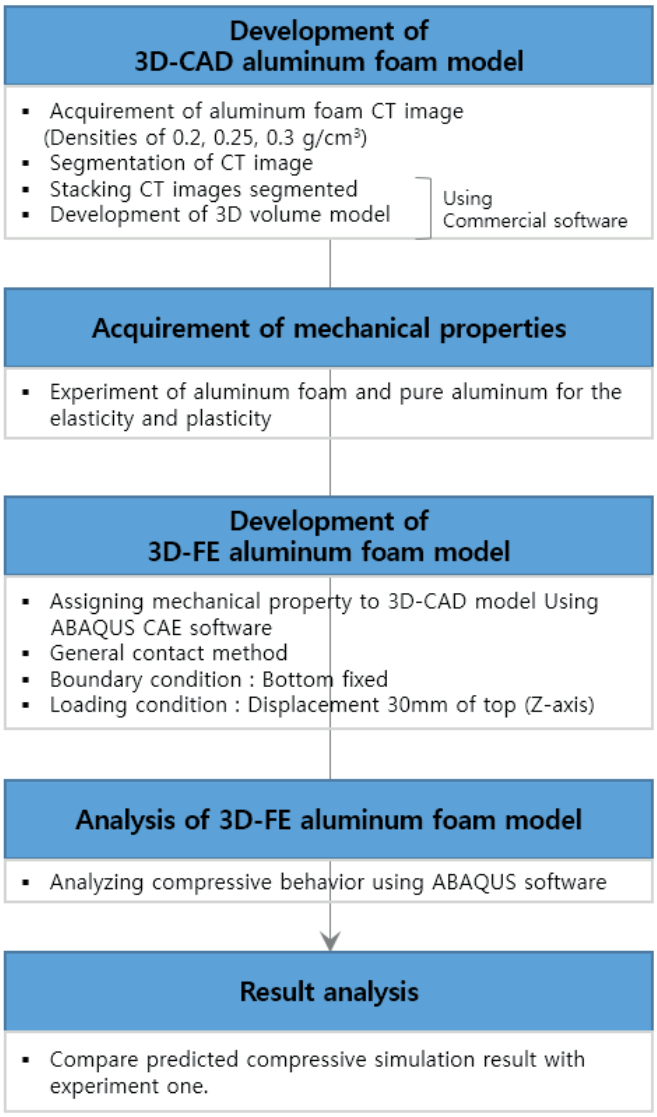

Fig. 4. Flow chart for modeling and analysis of aluminum foam

3. Results and discussion

Fig. 5 shows the compressive stress–strain curves of aluminum foams with densities of 0.2, 0.25, and 0.3 g/cm^3. For the aluminum foam with a density of 0.2 g/cm^3, the compressive strength was 0.6 MPa, and the plateau regime occurred in the strain range between 0.02 and 0.63. For the foams with densities of 0.25 and 0.3 g/cm^3, the compressive strength values were 1.83 MPa and 4.6 MPa, respectively. The plateau regime occurred in the strain range between 0.02 and 0.56 for the foam with a density of 0.25 g/cm3 and between 0.04 and 0.48 for the foam with a density of 0.30 g/cm3. According to Gibson et al. [13], the plateau regime is associated with collapse of the cell under compressive loading. When the cells of the foam material have almost collapsed, opposing cell walls touch, and further strain compresses the solid itself, producing the final region of rapidly increasing stress. Therefore, as the density increased, the range of the plateau regime decreased under compressive conditions.

The pore sizes of the aluminum foams with densities of 0.2, 0.25 and 0.3 g/cm^3 were studied using CT images. Fig. 6 shows the mean values and standard deviations of the aluminum foam pore sizes. For a density of 0.2 g/cm^3, the pore size is 13.4 mm and the standard deviation is ±6.32 mm. For densities of 0.25 g/cm^3 and 0.3 g/cm^3, the pore sizes are 10.76 mm and 7.65 mm, respectively, and standard deviations are ±3.9 mm, ±2.27 mm, respectively. As the density of the aluminum foam increased, the pore size and standard deviation decreased. These differences in pore size and standard deviation affect the compressive stress of aluminum foam.

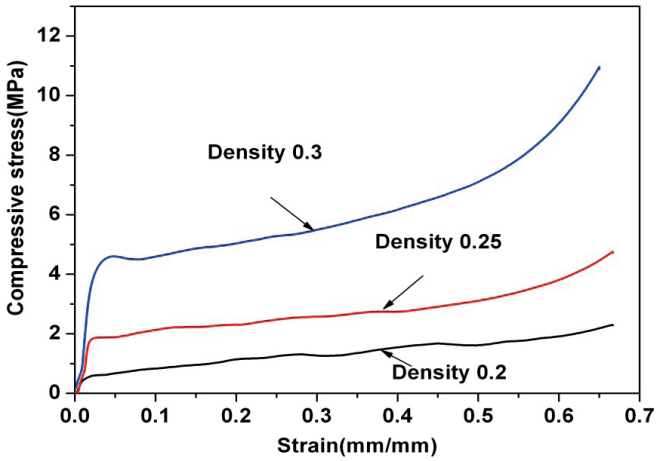

Fig. 5. Compressive stress-strain curves of aluminum foams for three densities

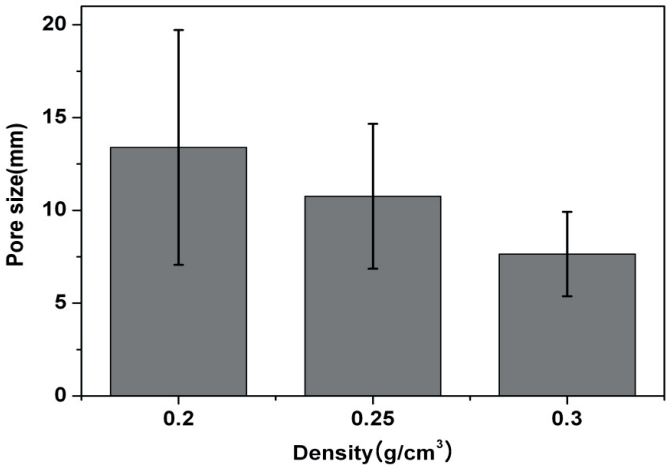

Fig. 6. Comparison of pore size for aluminum foams of three densities

Figs. 7–9 compare the predicted compressive stress–strain curves with those determined by experiments for the aluminum foam with densities of 0.2, 0.25, and 0.3 g/cm^3. For the foam with a density of 0.2 g/cm^3 in fig.7, the predicted compressive stress–strain curve showed a tendency similar to that of the experiment up to 0.5 strain. For the foams with densities of 0.25 and 0.3 g/cm^3, shown in Figs. 8 and 9, the predicted compressive stress–strain curves showed tendencies similar to those of the experiment up to 0.4 strain. In the 0.2 g/cm^3 case, the compressive strength determined from the analysis was higher than that determined from the experiment. However, in the 0.25 and 0.3 g/cm^3 cases, the predicted stress was higher than the experimental one after about 0.4 strain. The discrepancy in the compressive stress–strain curves in a high-strain range is associated with the

contact between the aluminum foam walls broken by the large deformation [13]. Also, the standard deviation of the aluminum foam pore size affected discrepancy of simulation results.

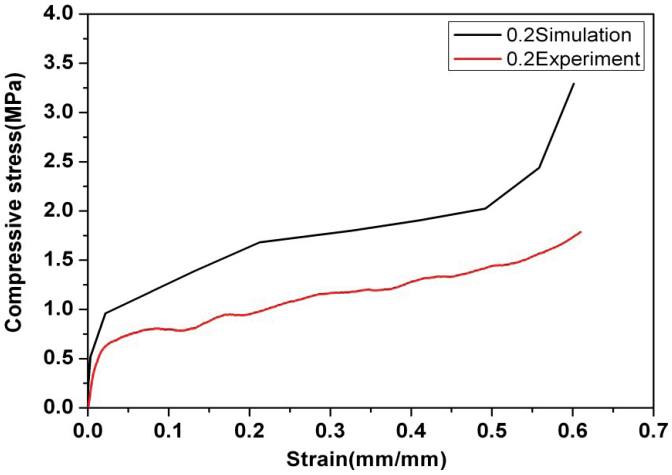

Fig. 7. Comparison of experimental and simulation compressive results for 0.2 g/cm3 density

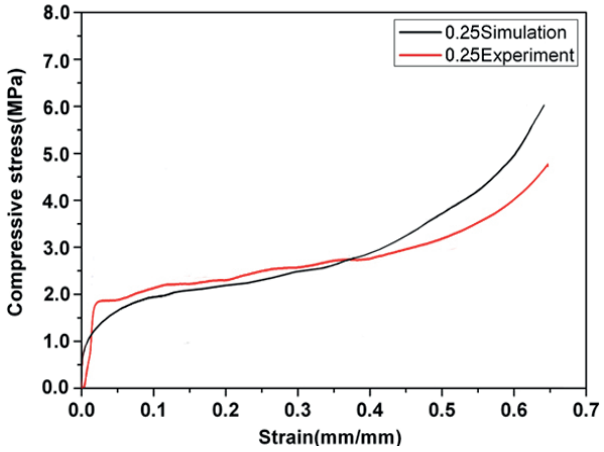

Fig. 8. Comparison of experimental and simulation compressive results for 0.25 g/cm3 density

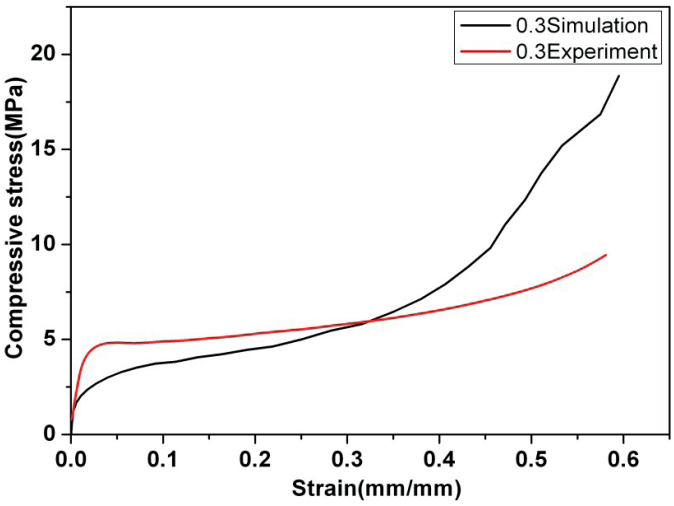

Fig. 9. Comparison of experimental and simulation compressive results for 0.3 g/cm3 density

Figs. 10–13 show the compressive deformation pattern of aluminum foams with densities of 0.2 and 0.3 g/cm^3 obtained by the experiment and the simulation by 3D FEA aluminum foam model. As shown in Figs. 10 and 12, the collapse of the actual aluminum foams was initiated at the top of the foam, and the collapse occurred from top to bottom. This deformation means that compressive energy was absorbed. Aluminum foam is broken from the top since the whole foam aluminum is not connected by pores of aluminum foam. Aluminum foam is a complex material in which metal walls and air are interconnected. Therefore, the compressive stress operates intermittently, not continuously, which breaks the aluminum foam from the top. The compressive simulation results (Figs. 11 and 13) showed deformation patterns similar to those of the experiment, i.e., the collapse of the 3D aluminum foam model was initiated at the top. The 3D model also collapsed from top to bottom, the same as seen in the experiments. Thus, the predicted deformation pattern agrees well with the experimental one within a certain range of strain. However, the discrepancy between the predicted and experimental deformation patterns increased as the strain increased. The reason is that many elements were distorted and had contact problems, which caused numerical errors. To overcome this problem, it is necessary to increase the computational capability, which would make it possible to refine the mesh and avoid elements with low aspect ratios.

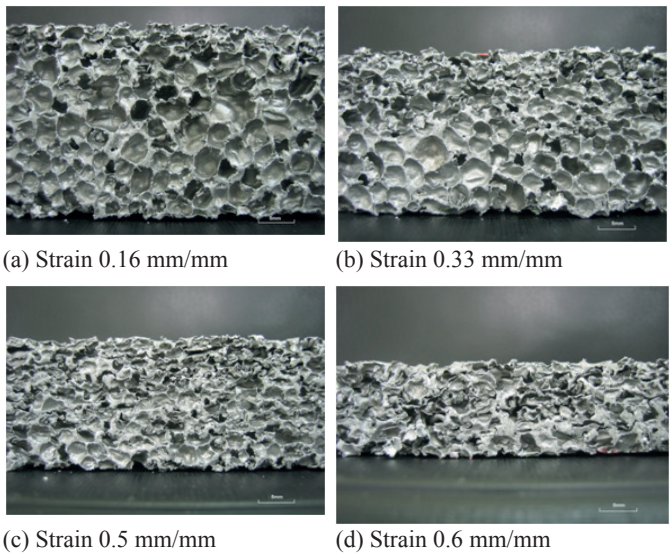

(a) Strain 0.16 mm/mm (b) Strain 0.33 mm/mm

(c) Strain 0.5 mm/mm (d) Strain 0.6 mm/mm

Fig. 10. Experimental results of aluminum foam compressive deformation (density 0.2 g/cm^3).

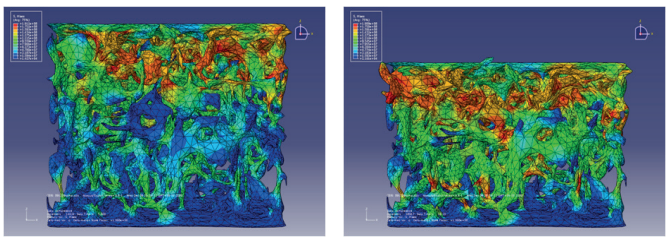

(a) Strain 0.16 mm/mm (b) Strain 0.33 mm/mm

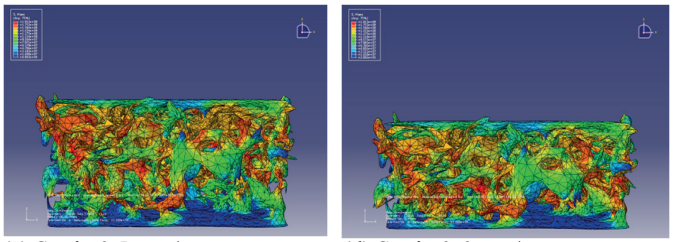

(c) Strain 0.5 mm/mm (d) Strain 0.6 mm/mm

Fig. 11. Simulation results of aluminum foam compressive deformation (density 0.2 g/cm^3)

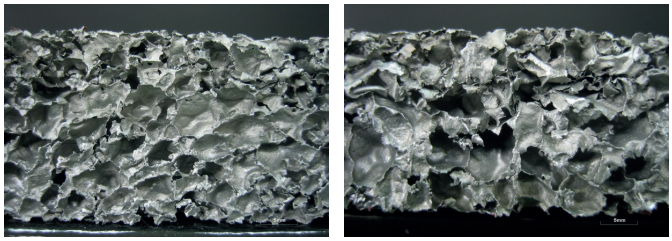

(a) Strain 0.16 mm/mm (b) Strain 0.33 mm/mm

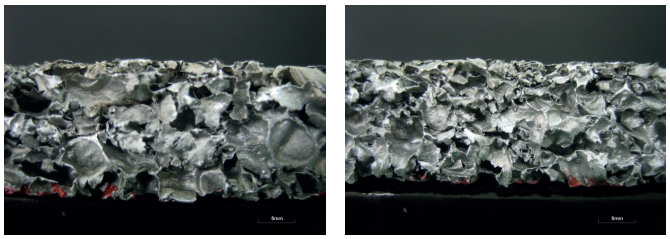

(c) Strain 0.5 mm/mm (d) Strain 0.6 mm/mm

Fig. 12. Experimental results of aluminum foam compressive deformation (density 0.3 g/cm3)

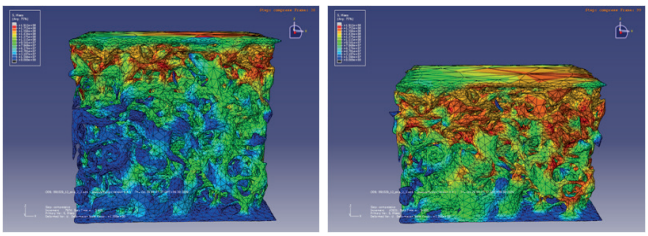

(a) Strain 0.16 mm/mm (b) Strain 0.33 mm/mm

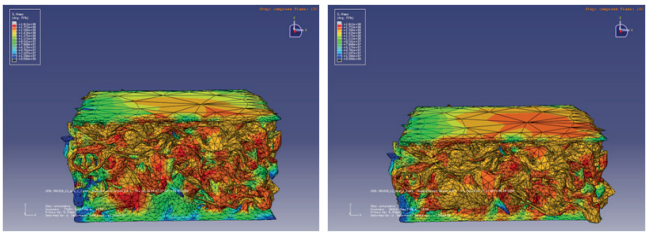

(c) Strain 0.5 mm/mm (d) Strain 0.6 mm/mm

Fig. 13. Simulation results of aluminum foam compressive deformation (density 0.3 g/cm^3).

4. Conclusions

In this study, numerical analysis on the compressive behaviors of aluminum foam with various densities was performed using a 3D aluminum foam model constructed from CT images. The predicted compressive behaviors were compared with those determined by the actual compressive tests. The conclusions obtained from this study are as follows. First, the predicted compressive stress–strain curves displayed tendencies similar to those determined from the experiment for the three densities. However, the compressive strengths determined from the analysis were higher than those determined from the experiment. The discrepancy of compressive behaviors between the analysis and the experiment is associated with the contact of the aluminum foam walls by deformation. The differences of real and predicted pore sizes affected the compressive simulation results of the aluminum foam. By developing an image processing method and meshing technique, the numerical model based on FEM seems to be appropriate for modeling foam materials.

Acknowledgments

This work was supported by the Basic Science Research Program through the National Research Foundation of Korea (NRF) funded by the Ministry of Education, Science and Technology (project number: 2013R1A1A2A10063466).

REFERENCES

[1] D.P. Mondal, M.D. Goel, S. Das, Compressive deformation and energy absorption characteristics of closed cell aluminum-fly ash particle composite foam, Materials Science and Engineering A **507**, 102-109 (2009).

[2] A.E. Markaki, T.W. Clyne, Energy absorption during failure of layered metal foam/ceramic laminates, Materials Science and Engineering A **323**, 260-269 (2002).

[3] S. Asavavisithchai, D. Slater, A.R. Kennedy, Effect of bonding strength on the energy absorption of al foam-filled cylindrical tube, Journal of Materials Science **39**, 5873-5875 (2004).

[4] C.S. Lee, D.G. Lee, Manufacturing of composite sandwich robot structures using the co-cure bonding method, Composite Structures **65**, 307-318 (2004).

[5] S. Santosa, J. Bangart, T. Wierzbicki, Bending crush resistance of partially foam-filled sections, Advanced Engineering Materials **2**, 223-227 (2000).

[6] S.P. Santosa, T. Wierzbicki, A.G. Hanssen, M. Langseth, Experimental and numerical studies of foam-filled sections, International Journal of Impact Engineering **24**, 509-531 (2000).

[7] P.S Liu, Tensile fracture behavior of foamed metallic materials, Materials Science and Engineering A **384**, 352-354 (2004).

[8] J. W. Hutchinson, M. Y. He, Buckling of cylindrical sandwich shells with metal foam cores, International Journal of Solids and Structures **37**, 6777-6794 (2000).

[9] A. Salimon, Y, Brechet, M.F. Ashby, A.L. Greer, Potential applications for steel and titanium metal foams, Journal of Materials Science **40**, 5793-5799 (2005).

[10] M.D. Demetriou, G. Duan, C. Veazey, K.D. Blauwe, W.L. Johnson, Amorphous Fe-based metal foam, Scripta Materialia **57**, 9-12 (2007).

[11] H.J. Chung, K.Y. Rhee, B.S. Han, Y.M. Ryu, Plasma treatment using nitrogen gas to improve bonding strength of adhesively bonded aluminum foam/aluminum composite, Journal of Alloys and Compounds **459**, 196-202 (2008).

[12] H.J. Chung, K.Y. Rhee, B.C. Lee, J.H. Lee, Effect of oxygen

plasma treatment on the bonding strength of CFRP/aluminum foam composite, Journal of Alloys and Compounds **481**, 214-219 (2009).

[13] L.J. Gibson, M.F. Ashby, Cellular solids, Pergamon Press, Oxford, UK, 2001.

[14] I.Ch. Konstantinidis, D.P. Papadopoulos, H. Lefakis, D.N. Tsipas, Model for determining mechanical properties of aluminum closed-cell foams, Theoretical and Applied Fracture Mechanics **43**,157-167 (2005).

[15] P. Kenesei, Cs. Kádár, Zs. Rajkovits, J. Lendvai, The influence of cell-size distribution on the plastic deformation in metal foams, Scripta Materialia **50**, 295-300 (2004).

[16] A. Sassov, E. Cornelis, D. van Dyck, Non-destructive 3D Investigation of metal foam microstructure, Material Wissenschaft and Werkstofftechnik **31**, 571-573 (2000).

[17] T. Ohgaki, H. Toda, M. Kobayashi, K. Uesugi, T. Kobayashi, M. Niinomi, T. Akahori, K. Makii, Y. Aruga, In-situ high-resolution x-ray CT observation of compressive and damage behavior of aluminum foams by local tomography technique, Advanced Engineering Materials **8**, 473-475 (2006).

[18] Y. Liu, W. Gong, X. Zhang, Numerical investigation of influences of porous density and strain-rate effect on dynamical responses of aluminum foam, Computational Materials Science, **91**, 223-230 (2014).